Cumulative Error Calibrating with Few Landmarks by Matching Human Activity for PDR Indoor Positioning

Yonglei Fan[1], Zhao Huang[2], Guangyuan Zhang[3*], Xijie Xu[1], Guangxia Yu[1], Stefan Poslad[1]

[1] *Queen Mary University of London, Mile End Road, London, E1 4NS, United Kingdom*
[2] *Northumbria University, Northumberland Road, Newcastle, NE1 8ST, United Kingdom*
[3] *Peking University, No. 60 Yannan Yuan, Beijing, China*

Abstract

Severe cumulative errors significantly limit the applicability and expansion of IMU-based indoor localization. A quantitative analysis is conducted showing the impact that heading estimation and step length estimation have on cumulative error. In response, this paper proposes a method that utilizes a few numbers of indoor landmarks to assist IMU localization. Specifically, a lightweight self-attention model is employed to classify behavioral sequences from training data, matching behaviors with landmarks to reconstruct indoor paths. By sequentially linking space-discrete landmarks through time-continuous behaviors, a spatially reconstructed path is formed within the building, assisting PDR in correcting heading directions based on the resemblance between newly predicted and existing paths. When an activity matches a landmark, the positioning estimate is recalibrated to align with the identified landmark, thereby rectifying cumulative errors. While doing heading estimation, a deep learning technique is applied to mitigate sensor yaw misalignment in the IMU data. The proposed indoor positioning method demonstrates exceptional performance.

Keywords

Indoor positioning, IMU, PDR, Human activities, Landmarks, Cumulative Error

1. Introduction

PDR suffers from serious cumulative errors (CE) which derive from the estimation of three parameters: heading, stride, and stride length. A lot of efforts have been made to diminish it. One way is to improve algorithms, like Kalman Filter(KF) [1], Particle Filter(PF) [2] , and Deep Learning(DP) [3]. Heading estimation and Step length are corrected by these methods. However the measuring error is persistent, later corrections are based on positions with bias causing CE constantly. It seems necessary to have additional source data to assist, which is another way out. Correspondingly, different sources of data, like Wi-Fi [4, 5], Bluetooth [6], vision [7], etc. are applied with PDR to improve the accuracy. And better results have been made by them. The problem is that there are unequal scale errors, which cost abundant efforts, in additional data. More devices are also required which makes PDR lose its conciseness.

Additional information from other resources is necessary for CE correction of PDR. Auxiliary methods relying on wireless communication require data scales in the tens of thousands, while visual approaches demand even higher computational power, resulting in substantial human and

Proceedings of the Work-in-Progress Papers at the 14th International Conference on Indoor Positioning and Indoor Navigation (IPIN-WiP 2024), October 14 - 17, 2024, Hong Kong, China

⋆ You should use this document as the template for preparing your publication. We recommend using the latest version of the CEURART style.

* Corresponding author.

Yonglei.fan@qmul.ac.uk (Y.Fan);Zhao.huang@northumbria.ac.uk (Z.Huang); guangyuan.zhang@pku.edu.cn (G. Zhang); xijie.xu@qmul.ac.uk (X.Xu); Guangxia.yu@qmul.ac.uk(G.Yu); Stefan.poslad@qmul.ac.uk(S.Poslad)

financial costs. To mitigate these issues and enhance the convenience of PDR localization, we propose a method that combines a small number of landmarks with the extraction of behavioral information from IMU. Based on this idea, the path inside a building and human activity information are excavated from IMU. For the majority of indoor human physical activities, directly determining the position determination and navigation of the whole body is not essential because we can quickly visually learn and memorize the space layout to find out where we are and how to get to another location. Monitoring human movements has many more indirect benefits, e.g., determining the quantity of human motion, building occupancy with respect to layout, optimizing human physical activities that are distributed, care in the community of less physically able people, etc. Firstly, a deep learning method is applied to mine the behavior characteristics in IMU data, such as stairs up and down, turning, walking, stopping, etc., and map them with landmarks. Then, the path inside the building is reconstructed by matching landmarks and the original PDR result. The reconstructed path can help PDR itself to correct the heading. The contributions of our work are as follows:

1. IMU data is used to extract behavior semantics based on a self-attention model we designed. And mapping the relationship between pedestrians' behaviors and landmarks inside the building is built. This mapping relationship can update the position to the specific waypoints in the PDR positioning process.
2. The intrinsic nature of CE lies in the high autocorrelation of step sequences. The segmentation of this correlation through truncated approaches in behavior recognition constitutes a pivotal strategy for mitigating the CE. Furthermore, we discern that within disparate behavioral intervals, the state of motion remains constant, and this equilibrium state exerts a lesser impact on the CE compared to the transitional phases of behavior states.
3. Classification models effectively avoid noise interference in the data, whereas regression models are more susceptible to yaw misalignment, making them difficult to fit accurately. Peak and valley detection are both applied based on a low-pass filter and cooperate with vertex and interval threshold to clean the interference points shown in Figure.6
4. We designed a landmarks-based calibrating (shifting reference point to a new location related to an activity waypoint change) PDR location system based on activity information extracted from IMU data, which can alleviate the accumulated PDR error by mining the path information and behavior semantics hidden in the data. We compared the other two classic data fusion methods, PDR+WiFi and XMU_PDR, resulting in a 26.8% increase in real-time positioning.

2. Related Work

Sensor yaw misalignment inherently contributes to each localization result, propagating through the system with subsequent measurement. This necessitates precise interval alignment to accurately determine the IMU's relative position with respect to the carrier. Techniques typically involve nonlinear and linear Kalman filters or multi-vector solutions, which impose significant computational loads [8-10]. Attitude error dynamics are leveraged to analyze this issue. The observability of yaw misalignment is assessed using Piecewise Constant Systems (PWCS) and Singular Value Decomposition (SVD) theory [11]. Furthermore, the observability of roll misalignment in high-speed motion scenarios is improved [12]. In [13], the author proposes a method to estimate the bias between the IMU and the carrier coordinate systems, considering IMU bias. The estimation problem is treated as a joint state and parameter estimation problem, resolved using an adaptive estimator system dependent on IMU measurements. Additionally, the effectiveness of bias estimation can be evaluated by identifying the bias between high-precision INS/GNSS and the IMU and carrier coordinate systems.

The localization algorithm follows a Markov process, where errors in previous results propagate and accumulate through successive measurements. PDR is chain positioning mode, and each estimation depends on the last result. With the chain last, the error will be accumulated [14, 15]. To solve this problem, D. Yan et al. [16] proposed a deep belief network (DBN) focusing on the periodicity of angular rate while walking, peak–valley angular velocity detection, and zero-cross detection. Based on biomechanical models, N. Perukhov. et al. [17] minimized the length estimation error. In [16, 18], authors all use peak detection to determine one step, and they made efforts to noise canceling of acceleration. Magnetometers and gyroscopes are used for heading estimation. M.Abadi. [19] tried to use deep learning to reduce the strong disturbance of Earth's magnetic field inside buildings. J.Tian

[20] designed an adaptive adjustment mechanism of filter parameters based on measurement quality assessment to improve the applicability of the method to different speeds and groups of people.

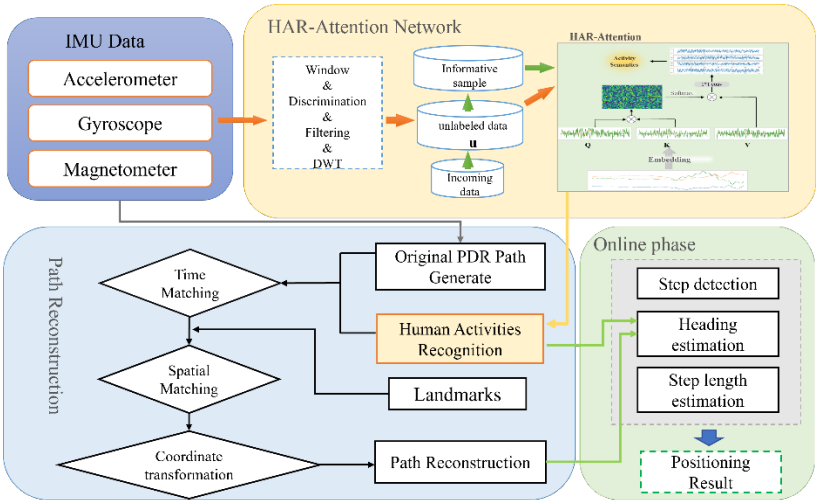

Figure 1. IMU fused with a few landmarks indoor positioning pipeline. The blue, orange, and blue parts are IMU data, data processing, and path reconstruction, and belong to the offline phase. The green part is the system testing which is the online phase.

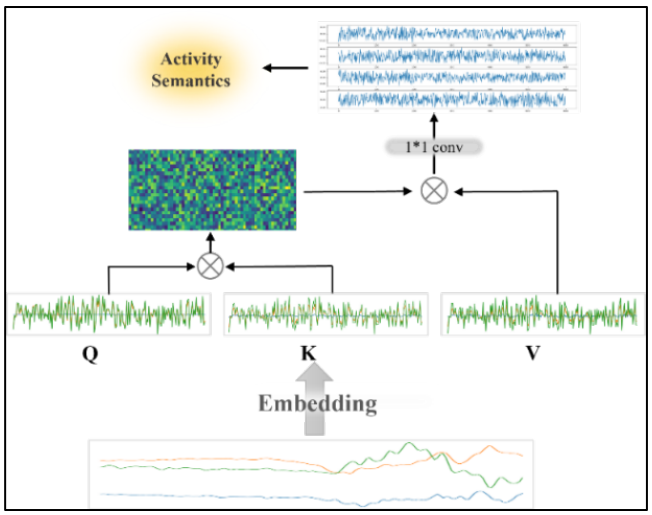

Figure 2. HAR self-attention network.

Additional data sources are also added to PDR to reduce the accumulated error. In [21, 22], authors use Wi-Fi to help PDR to improve its performance. Wi-Fi RSSI fingerprint provides a blurred area which corrects deviation in PDR. The same theory is employed in BLE [23, 24], RFID [25, 26], and UWB[27, 28]. The floor plan as another additional data source is also used to decrease error. Through the integration of data fusion, environmental data is procured to bolster PDR positioning by Ricardo Santos [29]. CE indeed requires additional information for correction, and a specific type of supplementary data limits the expansion of PDR across various data environments. Furthermore, IMU contains ample information that traditional PDR has not appropriately exploited. Based on these two key points, we propose a calibrating system based on the human physical activity information system.

3. Method

3.1 Framework

The envisioned system bifurcates into two distinct stages: the offline phase and the online phase. In the preliminary offline phase, depicted in the yellow and blue sections of the diagram, IMU data serves as the initial input, feeding into the "HAR-Attention Network" to extract pertinent human

behavior information. This data, once harvested, is synchronized with the traditional PDR outcomes in a temporal context. Subsequently, spatial matching of reference point coordinates with behavioral semantics ensues. Through a process of coordinate transformation, the original PDR results undergo a refined correction, culminating in the reconstitution of the indoor pathway, as illustrated in the blue segment of the figure. Progressing to the online phase, considerable rectification of the heading is realized, leveraging the meticulously reconstructed path. This stage involves the strategic resetting of the original PDR positioning at critical nodes, facilitated by the identification and alignment of specific behaviors. This intricate process ultimately yields real-time, high-accurate positioning results.

3.2 Self-attention HAR algorithm

The self-attention mechanism, a trailblazing concept, has gained considerable acclaim in the domain of natural language processing. When applied to serialized datasets, such as IMU data, which is rich in human activity insights, it uncovers a multitude of semantic modules. Capitalizing on this compatibility, our research harnesses the self-attention mechanism to delve into and elucidate the subtle semantic layers embedded within the activities represented in IMU data.

The Figure 2. illustrates the architecture of the model, with IMU data serving as the input which is initially subjected to a linear embedding. Utilizing an attention mechanism, the data undergoes a re-weighting process as delineated by the formula. This entails computing the dot-product results of the Q and K, which are subsequently multiplied by the matrix V, thereby channeling heightened focus toward regions with greater weighted significance, shown below:

$$Attention(Q, K, V) = softmax(\frac{QK^T}{\sqrt{d_k}})V \tag{1}$$

Where $\boldsymbol{Q} \in \mathbb{R}_{tq*dq}$, $\boldsymbol{K} \in \mathbb{R}_{tq*dq}$ and $\boldsymbol{V} \in \mathbb{R}_{tq*dq}$ are three inputs of the self-attention layer: queries, keys, and values, where tq, tk, and tv are the element numbers in different inputs and dq, dk, and dv denote the corresponding element dimensions. The scalar $\frac{1}{\sqrt{d_k}}$ prevents the Softmax function from falling into regions with tiny gradients. One query's output is computed as a weighted sum of the values, where each weight of the value is computed by a designated function of the query with the homologous key.

$$O = Attention * W^o, W^o \in \mathbb{R}^{\frac{C}{b}*C} \tag{2}$$

Where O represents the output of $1 * 1$ convolution layer weighted by W^o and the attention layer $Attention$. And the final output of this network is:

$$HAR_{result} = O * W^F_{Linear} \tag{3}$$

Where HAR_{result} is the recognition result, W^F_{Linear} represents the fully connected layer.

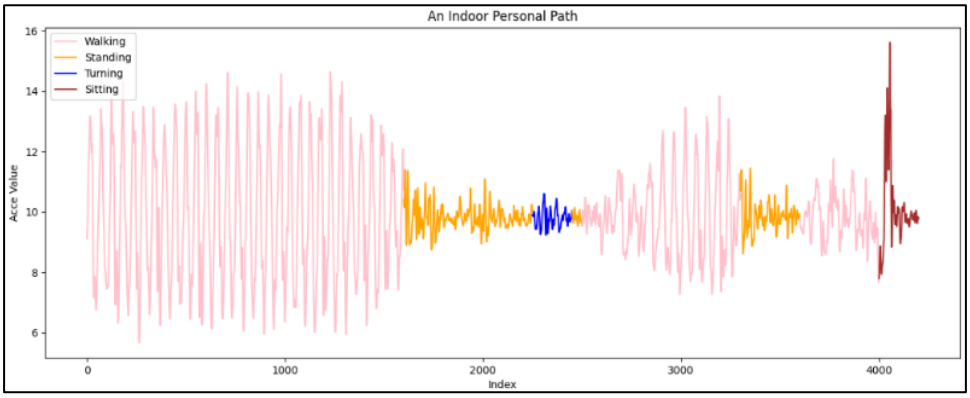

Figure 3: A simple example shows the self-attention HAR results in an indoor track of pedestrians.

We apply this network to some daily activity recognition, such as sitting down, walking, turning, turning back, and standing. Table 1. shows the result which is higher than some other models used by different research groups. Regarding certain intricate aspects of the models, as well as their analyses, due to their deviation from the main theme of this paper, they will not be elaborated upon further. In Figure 3., one example of the HAR result is visualized which reflects the behavior sequence in a simple path.

Table 1
The HAR comparison in different algorithms.

	Accuracy	Precision	Recall	F1-score
CNN	90.21%	88.72%	90.56%	89.63%
LSTM	88.63%	87.45%	85.94%	86.69%
SVM	93.97%	91.30%	92.00%	91.64%
Proposed	**96.37%**	**94.07%**	**96.52%**	**95.27%**

3.3 Reference path reconstruction

During the training phase, conventional PDR is used to generate the initial path which has a large cumulative error. Then, the timestamps of behavior recognition in section 3.2 are obtained to match the path nodes in the time domain. Afterward, coordinates transformations are made to the heading estimation of conventional PDR in different time periods based on known reference points.

Figure 4. (a) shows the path generated by conventional PDR, and the lower part shows the timestamps of different behavior results recognized by the 'self-attention network' in the time sequence. The time nodes of the behaviors are matched with the results of the generated path, resulting in the visualization of the matching results shown in (b), where the red markers represent the matching results. The indoor reference coordinates are used to correct the coordinate positions of the matches. The angle at which each behavior landmark deviates from the reference point is defined as the formula (4):

$$\theta = \arccos\left[\frac{(x_{pre},\, y_{pre})*(x_{ref},\, y_{ref})}{|(x_{pre},\, y_{pre})|*|(x_{ref},\, y_{ref})|}\right] \tag{4}$$

Where, the angle θ represents the angle between the original estimated point and the reference point. $(x_{pre},\, y_{pre})$ represents the estimated coordinates of PDR, and $(x_{ref},\, y_{ref})$ represents the coordinates of the reference position.

The deviation angle can be used to correct the predicted path of PDR. The formula for correcting each predicted point is as follows (5):

$$\begin{cases} x'_{pre} = y_{pre} * \sin\theta + x_{pre} * \cos\theta \\ y'_{pre} = y_{pre} * \cos\theta - x_{pre} * \sin\theta \end{cases} \tag{5}$$

Where (x'_{pre}, y'_{pre}) represents the coordinates after heading correction.

After performing heading conversion on all coordinates in each time interval, the reconstruction of the indoor path is completed, as shown in the result in Figure 4. (c).

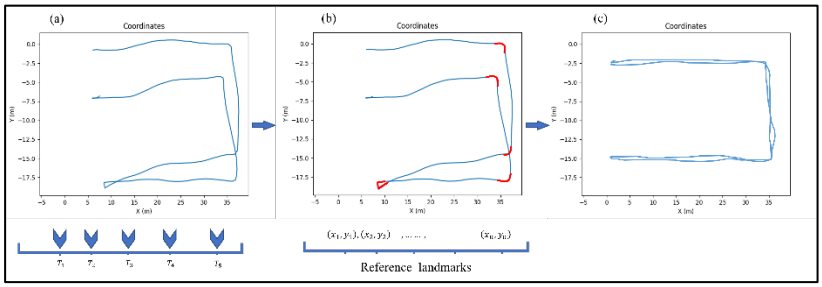

Figure 4. Indoor approximative path reconstruction process. In (a), the original path is constructed and at $\{T_1 \sim T_5\}$, five behavior is detected. Matching with the landmark in (b) and based on formulas (4) and (5), the approximative path is reconstructed.

3.4 Real-time landmarks-assist PDR indoor positioning system

3.4.1 Heading estimate

The main reason for the serious CE in conventional PDR is the deviation in heading estimation explained later. To avoid errors in heading estimation, the reconstructed path in the indoor environment is used as an effective basis for heading determination. The path between the behavior recognition points is classified as the same heading, and the reconstructed path data is sliced and

used as training samples. An MLP is used to fit the estimated heading with the training data, completing an accurate estimate of the heading. To reduce time complexity, we used lightweight weight parameters, with the number of nodes in each hidden layer being (40, 120, 30, 1). The structure of the MLP model is shown in Figure 5. The results show that the CE caused by heading estimation in this case is very small, which is explained correspondingly.

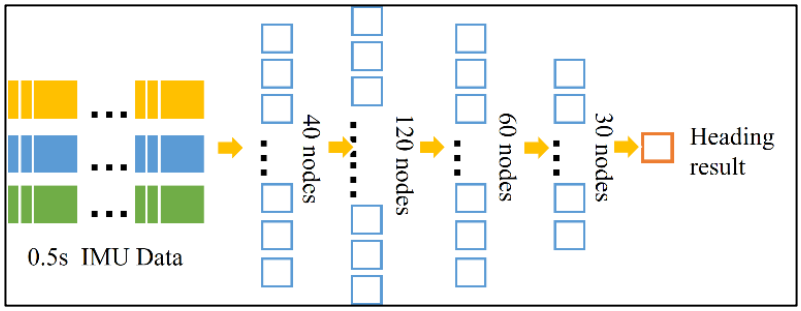

Figure 5. Heading Estimation Multilayer Perceptron

3.4.2 Step Detection

Step detection uses the regular dynamic changes of the accelerometer in the equipment on the three axes. This change is mainly reflected in that when one step is completed, the three-axis resultant force direction of the accelerometer will show a wave change pattern. It indicates that when one step is started, the accelerometer reading rises sharply, and at the end, the reading drops sharply. The sum values of the three-axis accelerometer measurement calculations are expressed as:

$$Acc_k = \sqrt[2]{AccX_k{}^2 + AccY_k{}^2 + AccZ_k{}^2} \tag{6}$$

where $AccX_k$, $AccY_k$, and $AccZ_k$ are the measurements from the three-axis accelerometers, and Acc_k denotes the sum values of these three-axis accelerometer measurements.

For this part, the main problem is to find out the peak value and valley accurately, and the peak value or valley value is exactly a complete gait. Due to the influence of noise, the traditional method can detect the peak value, but the peak value needs to be filtered twice, because the detected peak value always contains some interference, and these interference points are random. A low path filter is applied to straining high-frequency noise and the setting is:

$$W_n = \frac{F_c}{F_{nyq}} = 2 * \frac{F_c}{F_s} \tag{7}$$

Where F_c is the cut-off frequency, F_{nyq} is Nyquist frequency, F_s represents sampling rate and W_n is the Normalized cut-off frequency.

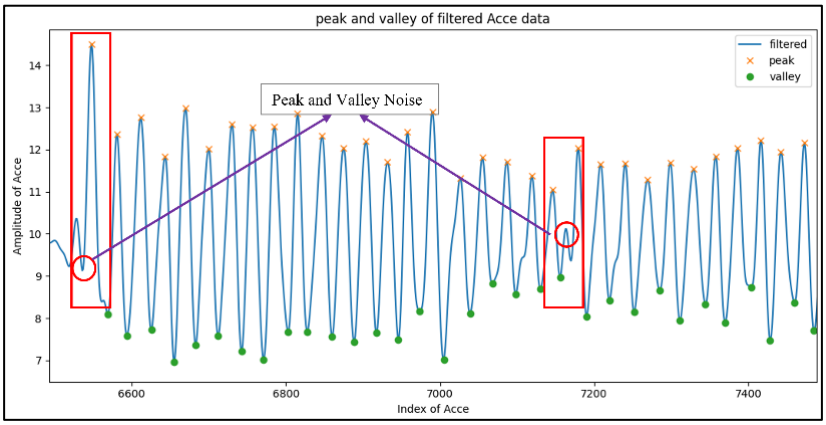

Figure 6. Peak and valley detection results in which the noises are filtered.

Peak and valley detection is then applied to the filtered accelerated data. There is also low-frequency noise caused by the physical shaking which will be also detected in peaks or valleys as shown in the red circle in Figure 6. To avoid this detection error, vertex, and interval threshold is used.

3.4.3 Step length estimation

Generally, a linear frequency model or empirical model is used to calculate the step length. The linear frequency model mainly uses height and step frequency to establish a linear relationship with

the step length. This method generally has low calculation cost, but a high error rate. At present, most of the step estimation methods using PDR for positioning generally use parametric models. The parametric model is proposed in this paper [30], using an empirical model.

Table 2.
The algorithm of CE calibrating with a Few landmarks system.

Algorithm 1: CE calibrating with a few landmarks system

Input: $\boldsymbol{P_{last}}$ (*position at last moment*), $\boldsymbol{v_{imu}}$ (*IMU data vector*)

Output: $\boldsymbol{P_{this}}$(*position at this moment*)

While $T_{now} \neq T_{end}$:

do Step Detection:

If True, **then**:

1: Load the Heading estimation model M_h

2: Load the Step length estimation model M_{s_l}

3: Get $\boldsymbol{v_{imu}}$ in real-time, the time slot is 0.5s

4: Calculate the Heading and Step length:

$H_e^k = M_h(\boldsymbol{v_{imu}})$, where H_e^k is the k_{th} estimated Heading.

$L_e^k = M_h(\boldsymbol{v_{imu}})$, where L_e^k is the k_{th} estimated Step length.

5: Update H_e based on Kalman Filter:

$$H_e^k = K * H_e^k + (1 - K) * \sum_i^n H_e^{k-i},$$

Where K is the coefficient which can reduce the impact of mutation values.

6: Update the position at this moment:

$$P_{this} = Geo(P_{last}, H_e^k, L_e^k),$$

Where $Geo()$ represents the Earth coordinate calculation algorithm.

End if

End while

$$step_{length} = c * \sqrt[4]{A_{max} - A_{min}} \tag{8}$$

Where A_{max}, A_{min} represent the maximum and minimum of accelerate, c is the rate index and it represents the influence of the high, step direction and step rate to step length.

Indeed, the precision of this method for estimating step length is notably inconsistent. This variability largely stems from the substantial oscillation in the differential between peak and trough values. As discernible from the equation, this fluctuation diminishes somewhat when raised to the fourth power. Nonetheless, even minor discrepancies, once magnified by the coefficient c, can result in significant deviations in step sizes. Conversely, employing the reconstructed path as a corrective measure for step estimation markedly enhances the stability, effectively mitigating the cumulative error in PDR attributable to inaccuracies in step calculations.

3.5 Real-time CE calibrating PDR system

The algorithm outline is shown in Table 2. If there is a new movement, the first step is to use low pass filtering and peak detection methods to process the accelerometer data, then update the peak point list and record the peak point time. Second, obtain the maximum and minimum values of the accelerometer within 0.2s before and after the peak point, and then calculate the step size. The third step is to estimate the heading using the data from the gyroscope, accelerometer, and magnetometer. Finally, return the location result and update the location.

4. Experiment and Result

The preceding chapter delineated the entire algorithmic workflow along with the intricacies of its

implementation. This section is dedicated to applying the algorithm across diverse datasets, collected from within various architectural structures, thereby substantiating the algorithm's efficacy.

4.1 Data analysis

The data is officially provided by IPIN 2021 and IPIN 2022 Conference. A variety of sensor data collected in mobile phones, such as Wi-Fi, BLE, light, sound, barometric pressure, acceleration, gyroscope, and magnetometer, are used to complete indoor positioning tasks in the IPIN 2022 Track 3 competition. The data used in this stage are mainly from barometers, accelerometers, gyroscopes, and magnetometers. Their data format is shown in the following Table 3. The sampling frequency of different sensors is different. The sampling frequency of the barometer is below 10Hz, and that of the accelerometer, gyroscope, and magnetometer is about 50Hz.

Table 3.
The format of the dataset [31].

MAGN: the local magnetic field, as measured by the 3-axis magnetometer in the phone	
Format	MAGE; AppTimestamps(s); SensorTimestamp(s); Mag_X(uT); Mag_Y(uT); Mag_Z(uT);
Example	MAGE; 0.0035;8902.708;-20.700;-34.02000;-19.20000;3
ACCE: the phone's acceleration, as measured by the 3-axis accelerometers in the phone	
Format	ACCE; AppTimestamps(s); SensorTimestamp(s); Acc_X(uT); Acc_Y(uT); Acc_Z(uT);
Example	ACCE; 0.0035;8902.708;-1.8004;6.41464;-7.17303;3
GYRO: measure the phone's rotation, as measured by the 3-axis magnetometer in the phone	
Format	GYRO; AppTimestamps(s); SensorTimestamp(s); Gyr_X(uT); Gyr_Y(uT); Gyr_Z(uT);
Example	GYRO;0.0035;8902.708;-0.22846;-0.22930;-19.20000;3
PRES: the atmospheric pressure	
Format	PRES; AppTimestamps(s); SensorTimestamp(s); Pres(bar); Accuracy(integer)
Example	PRES;0.0035;8902.708; 2.20000;3

In the process of data analysis, data over a long period is used to verify the effectiveness of the algorithm. For example, in gait detection algorithm, acceleration data up to ten minutes is used to test the effects of low-pass filtering and peak detection. The proposed algorithm is a real-time positioning algorithm, so it is necessary to specify how much of the positioning frequency is in real-time. Although, under different requirements, the requirements for "real-time" are different, and in human indoor activities, the positioning frequency of 2Hz and above can be considered as a real-time state.
Figure 7. shows the data collection process and the way to hold the device. The user may have done other realistic movements such as stopping, sitting, attending a phone call, taking an elevator, among others. The focus is more on office buildings as they cater to a larger audience, and moreover, the behavior of individuals in office spaces is more purposeful, meaning that the pathways are more organized.

4.2 Off-line stage

During the training phase, data collection is imperative for the test area. The self-attention mechanism is then applied to this training data, facilitating the extraction of behavioral information from the sequential data. Concurrently, PDR is employed to garner initial path information. Following this, a correlation is established between the behavioral data and key nodes, leading to further rectification of the path information. The corrected data, endowed with enhanced directional accuracy, significantly mitigates the cumulative error issue inherent in PDR. This process culminates in the creation of foundational data for the real-time positioning system, thereby enabling the provision of highly precise, real-time location services.

Figure 7. The way the user holds the device[31].

4.2.1 HAR in map

The training set for the self-attention model mentioned in the previous chapter was self-collected, with a sampling frequency identical to that of the current experiment. The crux lies in the fact that the input length of the training dataset is 200*3, encompassing only a single activity type. To augment the model's adaptability, the positioning of the activity within the sample is randomized. However, in real indoor settings, data is temporally continuous, necessitating a more precise demarcation of the boundaries between behavioral nodes to avert significant recognition errors. We have employed a sliding window technique to delineate these boundaries. The window's width is set to 30, with padding of zeros at both ends to fulfill the model's input requirements. It is pivotal to note that the width of the sliding window is contingent upon the sampling rate, and the specific range for this setting can be referenced from the following formula:

$$W_{win} \approx F_s / \max(F_m) \tag{9}$$

Where W_{win} denotes the width of the sliding window, $F_s$represents the sampling frequency, and F_m is the frequency of the movement, typically ranging from 0.6Hz to 1.5Hz. Utilizing the maximum value of the frequency ensures that the data within the sliding window is minimized, as an influx of additional data into the window could precipitate severe recognition inaccuracies.

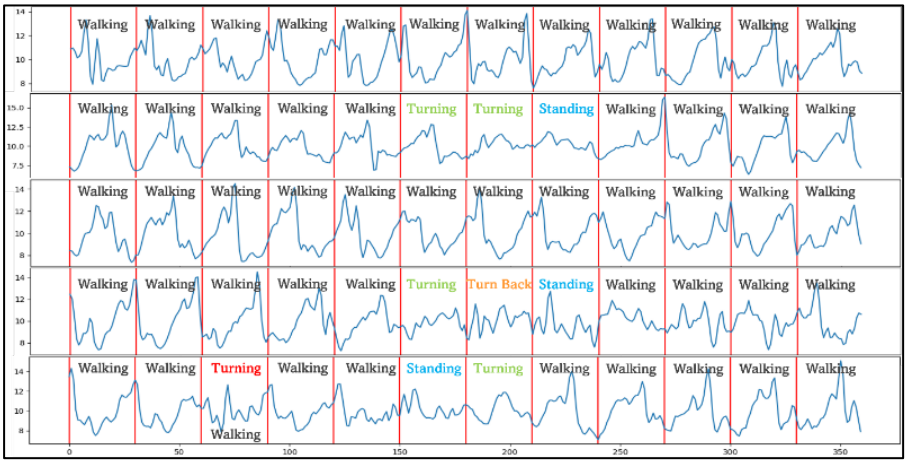

Figure 8. The results of 1 case of behavior recognition by the self-attention mechanism model.

Figure 8. showcases the results of behavior recognition by the self-attention mechanism model over a certain period with windows sizes 30 and 50. The blue curve in the diagram represents the variations in the accelerometer's modulus value throughout this process. Each pair of red lines demarcates the boundary of a window, within which data is sequentially fed into the model, resulting in the identification of behavioral categories. These categories are visually distinguished using text in various colors, with red font indicating samples that have been erroneously recognized. For these incorrectly identified instances, a heading consistency check is implemented.

Table 4. delineates the behavioral detection outcomes for three distinct paths, each collated from entirely separate buildings and varying in length. When the sliding window is set to 30 (W_{30})the accuracy rates for the three paths are 95.05%, 93.80%, and 95.18%, averaging at 94.85%. This is a mere 0.42% deviation from the training model's performance, indicating robust model resilience. However,

when the window length is increased to 50 (W_{50}) the accuracy rates plummet to 6.66%, 7.30%, and 9.24%, with an average of 7.69%. The rationale behind this steep decline is fairly evident: a longer window encompasses a more extensive range of movements, leading the model to misinterpret simple actions as complex ones.

Table 4:
The performance of behavioral detection with the windows size of 30 and 50.

Routs	Motion count	Errors (W_{30})	Accuracy	Errors (W_{50})	Accuracy
1	646	32	95.05%	603	6.66%
2	274	17	93.80%	254	7.30%
3	498	24	95.18%	452	9.24%
Average	1418	73	94.85%	1309	7.69%

4.2.2 Path in map

Utilizing conventional PDR, we initially generate a path, within which substantial cumulative errors are inherent. To rectify these errors to the greatest extent possible, we adopt the approach of aligning the serialized behavioral information, unearthed using the method mentioned in the previous subsection, with the original path on a time series basis. The ensuing Figure 9. serves as a case illustration. The top-left corner of the image represents a path generated by traditional PDR, with the top-right legend depicting an enlarged view of a turning point, which is the landmark, within the path. The lower sequence illustrates the behavioral detection results based on accelerometer data. We designate these specific points in the temporal domain as breakpoints and then effectively correct the heading direction from the previous breakpoint or origin to the current one. This strategy aims to minimize the CE caused by sudden directional changes during sustained activities. Moreover, the post-correction data provide a high-quality foundational basis for the heading estimation model.

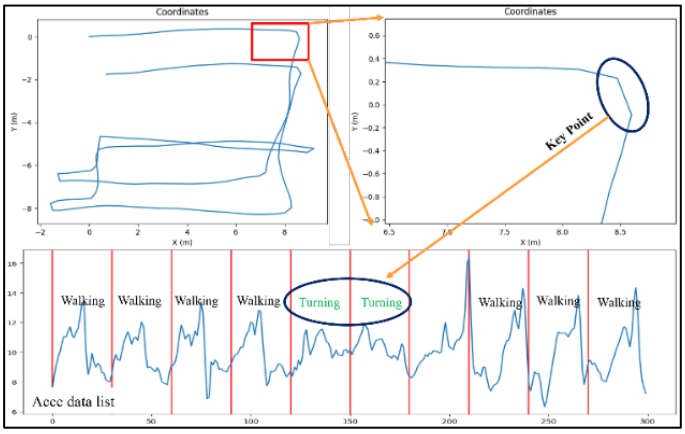

Figure 9. The way HAR results to correct the CE of PDR.

Figure 10. illustrates the efficacy of three reconstructed paths. The left side of the image presents a remote-sensing view of the building, highlighting the data collection path and the distribution of key points. These landmarks are sequenced to match the results of behavior recognition, followed by spatial corrections at the moments of these behaviors. Such adjustments are instrumental for both rectifying heading deviations and amending step length data during the process, which is crucial for reducing CE. The central green path diagram, generated by traditional PDR, shows a significant divergence from the actual path. This deviation tends to increase with each landmark encountered, thereby escalating the CE. The rightmost blue path diagram, after correction, contrasts with the green path by achieving substantial alignment adjustments, demonstrating a high degree of congruence with the original path.

The rectification of the indoor path map constitutes a pivotal step in generating more accurate sample data. This adjustment is not solely for the purpose of crafting a more precise map but also to cater to the demands of subsequent machine learning workflows. The resultant heading sample data

will serve as inputs for training the Multilayer Perceptron (MLP) model. These samples encapsulate the dynamics of movement within indoor environments, encompassing various positions and directions. The sample data is bifurcated into training and testing sets, utilized both for the training and the evaluation of the model's performance.

4.3 On-line stage

In the validation phase, the test paths involve data collection over extended durations, with the experimental setting situated within the intricate confines of an office building. This environment encompasses offices, corridors, conference rooms, and stairwells. The methodology for collecting validation data is consistent with the approach detailed in Section 4.1. For ground truth, we rely on GPS and laser rangefinders to obtain high-precision indoor location information, which is crucial for subsequent error assessments.

Figure 10. Three reconstructed paths and three columns are baselines, PDR result, and reconstructed path. *Note: All floor plans are showing the effect and were not used in the experiment.

Initially, we conducted an error analysis of the results, as depicted in the Cumulative Distribution Function (CDF) graph in Figure 11. which reveals that the method proposed here has improved the maximum error by approximately 8 meters, equating to a nearly 26.8% enhancement. Notably, in the initial phase, the steeper slope of the green line indicates that the overall errors are more densely clustered around smaller magnitudes. In contrast, the steeper sections of the orange and blue lines are observed in the latter half, suggesting that their errors are more prevalent in larger ranges. Within the CDF graph, the most significant discrepancy is at the median position, where the error corresponding to the green line is around 7 meters, compared to approximately 17 meters for the other two lines.

Subsequently, we visualized the results, as shown in Figure 12. The red path represents the data collection route, while the top-right orange path signifies the positioning results of the PDR algorithm. The bottom-left blue path indicates the PDR positioning outcomes augmented by the Kalman filter. The top-left green path represents the positioning results obtained using the proposed algorithm. From a visual standpoint, it is evident that both the traditional PDR and the Kalman filter-enhanced PDR algorithm exhibit significant deviations in heading calculations.

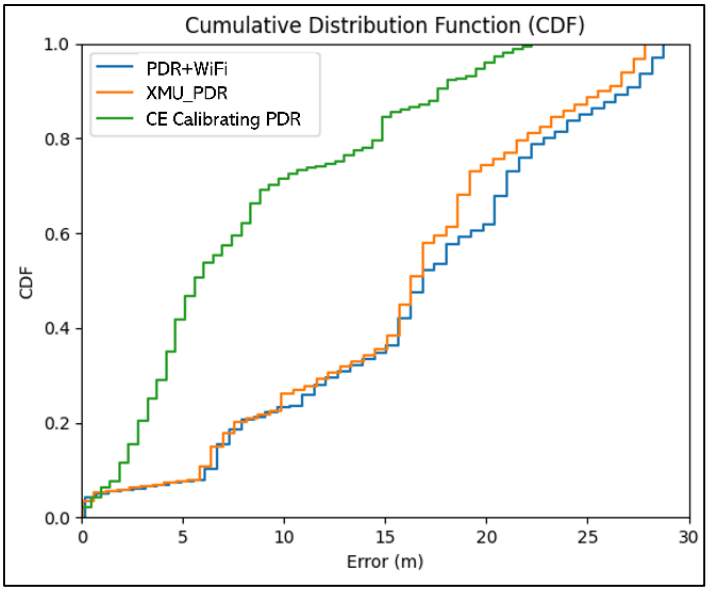

Figure 11. The CDF comparison between PDR + Wi-Fi, XMU_PDR, and the CE calibrating PDR.

To pinpoint the sources of error more accurately, we conducted separate assessments for heading and step length errors. As presented in Table 5., the total path length in the experimental data was 214.43 meters. The lengths computed by the three methods were 221.18m, 221.18m, and 215.01m, respectively. Both the PDR + Wi-Fi and XMU_PDR methods employed the same step length detection technique, resulting in identical total lengths for these two approaches. Their respective errors were 6.75m, 6.75m, and 0.68m, averaging out to an error of 0.01m, 0.01m, and 0.001m per step.

Concurrently, we quantified the errors in heading estimation with each position update. The Table 5. displays the total errors in heading determination across 677 position updates in this experiment, tallying to 30901.67, 17859.26, and 12693.75, respectively. The average error per update was 45.65, 25.38, and 18.75. The positional deviations caused by heading judgment errors with each position update were 0.26m, 0.15m, and 0.10m, respectively. Compared to the errors induced by step length estimation, the impact of heading determination errors on the results was more than 100 times greater. These statistics indicate that the primary source of CE is the misjudgment in the heading. Addressing this issue has been a focal point of our work.

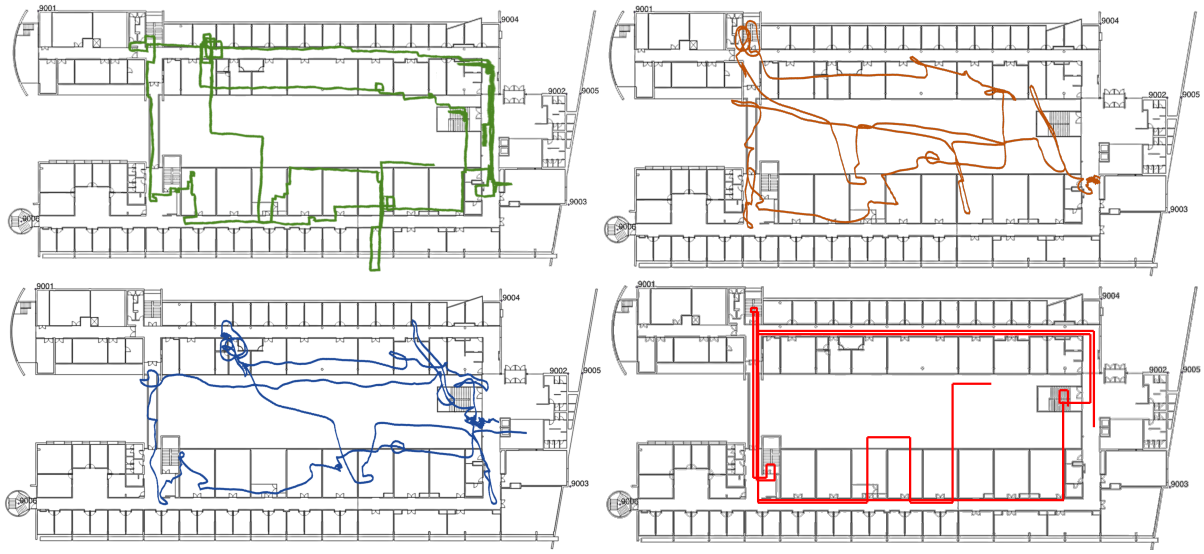

Figure 12. The visualization of layering the results on maps between PDR + Wi-Fi, XMU_PDR, and the Proposed. *Note: All floor plans are showing the effect and were not used in the experiment.

Table 5:
The quantitative error is caused by step length and heading estimation between different methods.

Method	Total length(m)	Error(m)	Error in step(m)	Sum heading error	Error for each step	Error by heading(m)
Initial path length	214.43	--	--			
PDR + Wi-Fi	221.18	6.75	0.01	30901.67	45.65	0.26
XMU_PDR	221.18	6.75	0.01	17859.26	25.38	0.15
Proposed	**215.01**	**0.68**	**0.001**	**12693.75**	**18.75**	**0.10**

5. Conclusion

In this study, we leverage the nuanced pedestrian behavior data and intrinsic path information within buildings to augment PDR positioning. This initiative heralds the advent of a few landmarks assisted, real-time PDR positioning system, adept at surmounting the traditional PDR's dependency on extraneous data for CE correcting. Former methodologies, which sought to rectify PDR's cumulative inaccuracies by amalgamating additional data sources, have significantly impeded PDR's evolution, predominantly due to the prohibitive costs and logistical complexities involved in data acquisition. Conversely, our approach of exploiting IMU data to substantially attenuate these cumulative errors represents a minimal investment with maximal yield, poised to catalyze the broader implementation of PDR. The proposed self-assisted PDR system is instrumental in enabling devices to ascertain real-time locations, thereby facilitating location-based services for users, given that IMU data invariably mirrors the motion state of its carriers. To enhance the precision of indoor path reconstruction, we employ multiple reference coordinate points as aids. While this method markedly elevates accuracy, it concurrently diminishes the system's autonomy. The rich tapestry of motion-related information encapsulated within IMU data is a boon to PDR's real-time positioning capabilities, necessitating advanced processing and extraction techniques. Moreover, the exploration of latent information within IMU data remains a paramount focus of our future endeavors.
Our application scenario, predominantly within office buildings, presents unique challenges. The diverse architectural layouts of different building types necessitate a broader spectrum of behaviors to adapt to varying contexts. Thus, validating and enhancing the algorithm's adaptability in such multifaceted environments is a primary objective we aim to pursue moving forward.

References

[1] X. Liu *et al.*, "Kalman filter-based data fusion of Wi-Fi RTT and PDR for indoor localization," *IEEE Sensors Journal,* vol. 21, no. 6, pp. 8479-8490, 2021.
[2] M. Sun, Y. Wang, S. Xu, H. Cao, and M. Si, "Indoor positioning integrating PDR/geomagnetic positioning based on the genetic-particle filter," *Applied Sciences,* vol. 10, no. 2, p. 668, 2020.
[3] S. Jeong, J. Min, and Y. Park, "Indoor positioning using deep-learning-based pedestrian dead reckoning and optical camera communication," *IEEE Access,* vol. 9, pp. 133725-133734, 2021.
[4] D. Yu, C. Li, and J. Xiao, "Neural Networks Based WiFi/PDR Indoor Navigation Fusion Methods," *IEEE Transactions on Instrumentation and Measurement,* 2022.
[5] Y. Lu, S. Luo, Z. Yao, J. Zhou, S. Lu, and J. Li, "Optimization of Kalman Filter Indoor Positioning Method Fusing WiFi and PDR," in *Human Centered Computing: 7th International Conference, HCC 2021, Virtual Event, December 9–11, 2021, Revised Selected Papers*, 2023: Springer, pp. 196-207.
[6] X. Wang *et al.*, "Tightly-Coupled Integration of Pedestrian Dead Reckoning and Bluetooth Based on Filter and Optimizer," *IEEE Internet of Things Journal,* 2022.
[7] M. Shu, G. Chen, Z. Zhang, and L. Xu, "Accurate Indoor 3D Location Based on MEMS/Vision by Using A Smartphone," in *2022 IEEE 12th International Conference on Indoor Positioning and Indoor Navigation (IPIN)*, 2022: IEEE, pp. 1-8.
[8] Z. Feng, X. Jiangning, and X. Cai, "A analytic coarse alignment method for SINS based on two-step recursive least squares," in *2015 Chinese Automation Congress (CAC)*, 2015: IEEE, pp. 2100-2105.

[9] C. Tan, X. Zhu, Y. Su, Y. Wang, Z. Wu, and D. Gu, "A new analytic alignment method for a SINS," *Sensors,* vol. 15, no. 11, pp. 27930-27953, 2015.
[10] Y. Zhang, L. Luo, T. Fang, N. Li, and G. Wang, "An improved coarse alignment algorithm for odometer-aided SINS based on the optimization design method," *Sensors,* vol. 18, no. 1, p. 195, 2018.
[11] X. Xia *et al.*, "Estimation on IMU yaw misalignment by fusing information of automotive onboard sensors," *Mechanical Systems and Signal Processing,* vol. 162, p. 107993, 2022.
[12] Y. Hwang, Y. Jeong, I. S. Kweon, and S. Choi, "Online misalignment estimation of strapdown navigation for land vehicle under dynamic condition," *International Journal of Automotive Technology,* vol. 22, pp. 1723-1733, 2021.
[13] V. Rodrigo Marco, J. Kalkkuhl, J. Raisch, and T. Seel, "A novel IMU extrinsic calibration method for mass production land vehicles," *Sensors,* vol. 21, no. 1, p. 7, 2020.
[14] D. Sato and N. Togawa, "A PDR Method Using Smartglasses Reducing Accumulated Errors by Detecting User's Stop Motions," in *2022 IEEE International Conference on Consumer Electronics (ICCE)*, 2022: IEEE, pp. 1-2.
[15] S. Wen *et al.*, "Enhanced Pedestrian Navigation on Smartphones with VLP-Assisted PDR Integration," *IEEE Sensors Journal,* 2023.
[16] D. Yan, C. Shi, and T. Li, "An improved PDR system with accurate heading and step length estimation using handheld smartphone," *The Journal of Navigation,* vol. 75, no. 1, pp. 141-159, 2022.
[17] N. I. Petukhov, V. N. Zamolodchikov, A. P. Malyshev, T. A. Brovko, S. A. Serov, and I. V. Korogodin, "Synthesis of PDR Algorithm and Experimental Estimation of Accuracy of Step Length Estimation Methods," in *2022 4th International Youth Conference on Radio Electronics, Electrical and Power Engineering (REEPE)*, 2022: IEEE, pp. 1-5.
[18] Y. Yang, B. Huang, Z. Xu, and R. Yang, "A Fuzzy Logic-Based Energy-Adaptive Localization Scheme by Fusing WiFi and PDR," *Wireless Communications and Mobile Computing,* vol. 2023, 2023.
[19] M. J. Abadi, L. Luceri, M. Hassan, C. T. Chou, and M. Nicoli, "A collaborative approach to heading estimation for smartphone-based PDR indoor localisation," in *2014 International conference on indoor positioning and indoor navigation (IPIN)*, 2014: IEEE, pp. 554-563.
[20] J. Tian, L. Cong, and H. Qin, "A PDR Heading Estimation Method Based on Motion Mode Recognition Using Adaptive UKF," in *2022 IEEE 12th International Conference on Indoor Positioning and Indoor Navigation (IPIN)*, 2022: IEEE, pp. 1-8.
[21] Z. Li, L. Zhao, C. Qin, and Y. Wang, "WiFi/PDR integrated navigation with robustly constrained Kalman filter," *Measurement Science and Technology,* vol. 31, no. 8, p. 084002, 2020.
[22] Y. Wu, R. Chen, W. Fu, W. Li, H. Zhou, and G. Guo, "Indoor positioning based on tightly coupling of PDR and one single Wi-Fi FTM AP," *Geo-spatial Information Science,* vol. 26, no. 3, pp. 480-495, 2023.
[23] X. Kong, C. Wu, Y. You, Z. Lv, and Z. Zhao, "Hybrid Indoor Positioning Method of BLE and Monocular VINS Based Smartphone," *IEEE Transactions on Instrumentation and Measurement,* 2023.
[24] M. Wang, N. Duan, Z. Zhou, H. Qiu, X. Li, and F. Zheng, "Indoor localization on smartphone using pdr and sparse deployed ble beacons in large open area," in *2021 International Wireless Communications and Mobile Computing (IWCMC)*, 2021: IEEE, pp. 141-148.
[25] V. Chand and J. Karthikeyan, "RFID-GPS based mechanism using aodvrp for stolen vehicle detection in VANET," *Indonesian Journal of Electrical Engineering and Computer Science,* vol. 18, no. 1, pp. 396-404, 2020.
[26] C. Zhao, Z. Li, H. Ding, G. Wang, W. Xi, and J. Zhao, "RF-Wise: Pushing the Limit of RFID-based Sensing," in *IEEE INFOCOM 2022-IEEE Conference on Computer Communications*, 2022: IEEE, pp. 1779-1788.
[27] G. T. Lee, S. B. Seo, and W. S. Jeon, "Indoor localization by Kalman filter based combining of UWB-positioning and PDR," in *2021 IEEE 18th Annual Consumer Communications & Networking Conference (CCNC)*, 2021: IEEE, pp. 1-6.
[28] L. Giarré, F. Pascucci, S. Morosi, and A. Martinelli, "Improved PDR localization via UWB-anchor based on-line calibration," in *2018 IEEE 4th International Forum on Research and Technology for Society and Industry (RTSI)*, 2018: IEEE, pp. 1-5.
[29] R. Santos *et al.*, "Crowdsourcing-based fingerprinting for indoor location in multi-storey buildings," *Ieee Access,* vol. 9, pp. 31143-31160, 2021.
[30] Z. Tian, Y. Zhang, M. Zhou, and Y. Liu, "Pedestrian dead reckoning for MARG navigation using a smartphone," *EURASIP Journal on Advances in Signal Processing,* vol. 2014, pp. 1-9, 2014.
[31] F. Potortì *et al.*, "Offsite evaluation of localization systems: criteria, systems and results from IPIN 2021-22 competitions," *IEEE Journal of Indoor and Seamless Positioning and Navigation,* 2024.